Available online at www.sciencedirect.com
SCIENCE DIRECT®
Physics of the Earth and Planetary Interiors 150 (2005) 265–286
PHYSICS OF THE EARTH AND PLANETARY INTERIORS
www.elsevier.com/locate/pepi

Reliability of geomagnetic paleointensity data: the effects of the NRM fraction and concave-up behavior on paleointensity determinations by the Thellier method

Annick Chauvin[a,*], Pierrick Roperch[b], Shaul Levi[c]

[a] *Géosciences Rennes, CNRS–Université de Rennes1 UMR 6118, Campus de Beaulieu Bat.15, CS74205, 35042 Rennes Cedex, France*
[b] *IRD, University of Chile, Santiago, Chile*
[c] *College of Oceanographic and Atmospheric Sciences, Oregon State University, Corvallis, OR 97331, USA*

Received 18 February 2004; received in revised form 3 November 2004; accepted 26 November 2004

Abstract

To test the reliability of the Thellier method for paleointensity determinations, we studied six historic lavas from Hawaii and two Gauss-age lava flows from Raiatea Island (French Polynesia). Our aim is to investigate the effects of the NRM fraction and concave-up behavior of NRM–thermal remanent magnetization (TRM) diagrams on paleointensity determinations. For the Hawaiian samples, the paleointensity results were investigated at both sample and site levels. For consistency and confidence in the paleointensity results, it is important to measure multiple samples from each cooling unit. The results from the Raiatea Island samples confirm that reliable paleointensities can be obtained from NRM–TRM diagrams with concave-up curvature, provided the data are accompanied by successful partial TRM (pTRM) checks and no significant chemical remanent magnetization (CRM) production. We conclude that reliable determinations of the paleofield strength require analyses of linear segments representing at least 40–50% of the total NRM. This new criterion has to be considered for future studies and for evaluating published paleointensities for calculating average geomagnetic field models. Using this condition together with other commonly employed selection criteria, the observed mean site paleointensities are typically within 10% of the Definitive Geomagnetic Reference Field (DGRF). Our new results for the Hawaii 1960 lava flow are in excellent agreement with the expected value, in contrast to significant discrepancies observed in some earlier studies.

Overestimates of paleointensity determinations can arise from cooling-rate dependence of TRM acquisition, viscous remanent magnetization (VRM) at elevated temperatures, and TRM properties of multidomain (MD) particles. These outcomes are exaggerated at lower temperature ranges. Therefore, we suggest that, provided the pTRM checks are successful and there is no significant CRM production, it is better to increase the NRM fraction used in paleointensity analyses rather than to maximize correlation coefficients of line segments on the NRM–TRM diagrams.

We introduce the factor, $Q = N\langle q\rangle$, to assess the quality of the weighted mean paleointensity, H_w, for each cooling unit.

Keywords: Paleointensity; Thellier method; Earth magnetic field; Paleomagnetism

* Corresponding author. Tel.: +33 2 23 23 60 92; fax: +33 2 23 23 60 90.
E-mail address: Annick.Chauvin@univ-rennes1.fr (A. Chauvin).

0031-9201/$ – see front matter © 2004 Elsevier B.V. All rights reserved.
doi:10.1016/j.pepi.2004.11.008

1. Introduction

Thermal remanent magnetization (TRM) is the only magnetization that can be used for obtaining absolute paleointensities of the Earth's magnetic field, and TRM in igneous rocks is the only recorder of absolute paleointensities prior to about 10,000 years ago (Perrin and Schnepp, 2004). The Thellier method (Thellier and Thellier, 1959) remains the most reliable and frequently used procedure (Valet, 2003). It is based on specific properties of TRM, mainly the linear dependence of TRM intensity on the inducing field and the additivity and independence of partial-TRMs (pTRMs). These properties are exhibited by populations of non-interacting single-domain (SD) grains but not by multidomain (MD) or pseudo-single domains (PSD) particles (Levi, 1977; Dunlop and Özdemir, 1997). Thelliers' technique requires that the samples be heated gradually in steps from room temperature to the Curie point. Together with the use of pTRM checks, the Thellier method makes it possible to detect the onset-temperature of modifications of TRM characteristics of the samples, caused by physico/chemical alterations of the magnetic minerals. Changes of TRM properties at higher temperatures lead to non-linear behavior of the NRM–TRM diagrams, failure of pTRM checks, and/or acquisition of chemical remanent magnetizations (CRM) that can be detected in the orthogonal demagnetization diagrams. Such changes often lead either to outright rejection of samples or the selection of a restricted temperature interval for calculating the paleointensity, where non-linearities and changes in TRM acquisition capacity can be neglected. Because significant mineralogical changes and TRM modifications during the Thellier procedure are more likely to occur at higher experimental temperatures, the paleointensity is frequently obtained from lower unblocking temperatures, where the NRM–TRM diagrams are substantially linear. In one of the most detailed paleointensity studies at the Steens Mountains volcanics (Prévot et al., 1985), there is evidence for unreliable results obtained from lower temperatures. In volcanic sequences, it is often the case that several successive lava-flows record indistinguishable paleomagnetic directions, which are treated as a distinct directional group. In the Steens Mountains study, the directional group DG46 comprises flows with reverse polarity, magnetized before a reversal, whereas the normal flows from directional group DG13 were extruded after the reversal. High paleointensities were found in flows from group DG13, and for this reason Prévot et al. (1985) argued that the field was more unstable after the transition. In Fig. 1, paleointensity estimates on samples from the DG46 and DG13 directional groups are plotted versus the NRM fraction used to determine the paleointensity. While the paleointensity data from DG46 were determined with low to high NRM fraction, only low NRM fraction was used for DG13. One possible interpretation of the results is that the high paleointensities determined with less than 30% of the NRM might be unreliable.

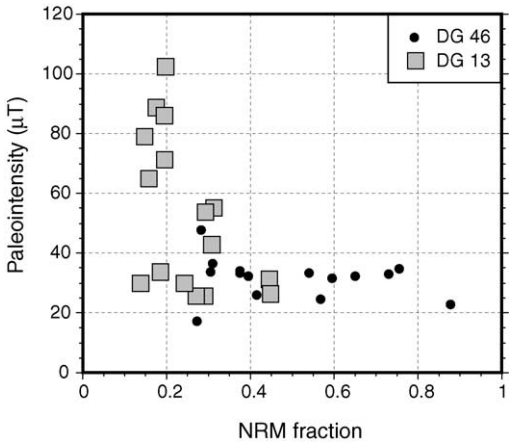

Fig. 1. Paleointensities for two directional groups: DG46 (reverse) and DG13 (normal) from the Steens Mountains (Prévot et al., 1985) vs. the NRM fraction used for the calculations. DG46: relatively little variation of field strength is observed when more than 30% of the NRM was used, while for DG13 paleointensities vary from 20 to 100 μT when using less than 20% of the NRM.

Calvo et al. (2002) studied six recent lava flows from Mt. Etna. They applied the following reliability checks of the Thellier method: (i) a minimun of four points in the NRM–TRM segment; (ii) NRM fraction equal or greater than 0.15; (iii) negligible secondary magnetization; (iv) differences between original pTRM and pTRM checks less than 15%; (v) differences between the slopes of the segments of the NRM–TRM curves between T_{max} and T_{check} before and after the pTRM check less than 15%. Calvo et al. (2002) obtained successful paleointensity results from only 6 of 28 samples, and the mean value was about 25% higher than the expected known field.

We conducted Thellier experiments on NRM carried by six historical lava flows from Hawaii and two from

Raiatea Island. The primary goal of this research is to achieve a broader understanding of factors that influence the reliability of absolute paleointensity determinations by the Thellier method, and to provide further guidelines for interpreting NRM–TRM diagrams.

2. Paleomagnetic sampling and methodology

On the island of Hawaii, we drilled between 7 and 16 standard, 25.4 mm diameter, cores from six recent flows (AD 1950, 1955, 1960, 1972, 1977, and 1982) (Fig. 2). On Raiatea Island (French Polynesia) 38 lavas were sampled with an average of seven cores per flow. The ages of these lava flows are between 2.44 and 2. 75 Ma (Duncan and McDougall, 1976; Blais et al., 1997). Because these units have normal polarity, their ages are likely to be older than 2.6 Ma.

Most samples were oriented with both magnetic and sun compass and during sampling, the vertical coverage of the lava flows was maximized (Tanaka and Kono, 1991; Biggin et al., 2003).

All cores were cut to 22 mm long cylindrical specimens. Progressive alternating fields (AF) demagnetizations were performed on one specimen from each core. Thellier paleointensity determinations were performed on 5–7 specimens from each flow at the paleomagnetic laboratories of Rennes and Oregon State University. Laboratory fields of 40 and 35 μT were applied during the experiments. Most of the samples were heated in air at low pressures ($<10^{-2}$ Torr) and a few at 1 atm.

Although the procedure proposed by Coe (1967), where the first heating is performed in zero field, is very popular, we prefer the original Thellier method (Thellier and Thellier, 1959) where both heatings are done in the laboratory field, reversing the field (or inverting the specimen) between the first and second heating. In this way, CRM with unblocking temperatures higher than the temperature of the chemical transformation will be more easily detected in the orthogonal demagnetization diagrams (Chauvin et al., 1991).

Furthermore, Yu et al. (2004) demonstrated that only the Thellier method is independent of the direction of laboratory field and detects reciprocity better than other techniques. We use the following procedures for pTRM checks: after the two heatings to T_i in opposite fields, we calculate the remaining NRM and the acquired pTRM $[T_i - T_0]$. The pTRM check at a lower temperature $T_j < T_i$ is performed in a field of opposite

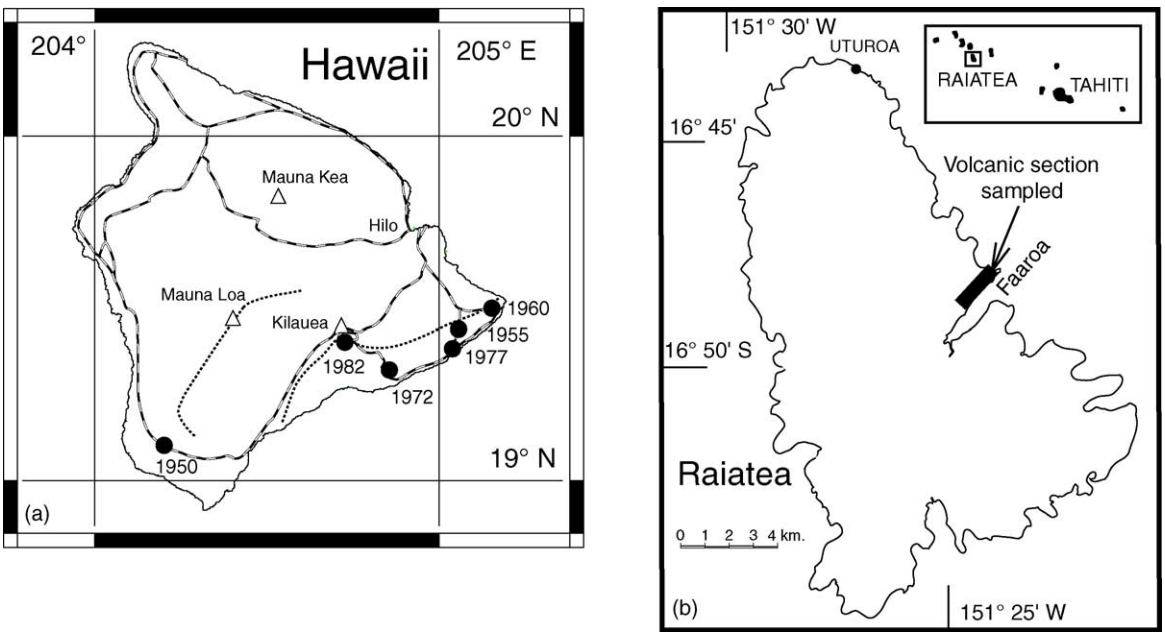

Fig. 2. Location map of (a) the six historical lava flows from Hawaii and (b) the volcanic section sampled in Raiatea Island.

direction to the second heating at T_i. The pTRM check at $T_j < T_i$ is simply half the difference of the magnetization measured after the second step at T_i and the magnetization measured after heating/cooling at $T_j < T_i$ in the opposite field. We agree with Yu et al. (2004) that pTRM checks are essential for detecting alterations of specimens during the experiment and should be required in all modern paleointensity investigations. We consider that the original in-field Thellier double heating procedure is the true optimal paleointensity (TOP) method.

3. Paleomagnetic directions

Characteristic directions were determined with linear least squares fit through the origin for both AF and thermal demagnetizations obtained during the paleointensity experiments.

For the historical Hawaiian flows, the expected direction from Definitive Reference Field (DGRF) model is about Dec = 11° and Inc = 37°. The mean direction for the six flows, Dec = 11.8°, Inc = 34.5°, and $\alpha_{95} = 3.1°$ (Table 1), is very close to the expected direction. Three flows H1960, H1977, and H1982 form a very tight directional group with Dec = 13.4°, Inc = 37.4°, and $\alpha_{95} = 1.0°$, indistinguishable from the DGRF (Table 1). However, a small negative inclination anomaly is recorded by flows H1950, H1955, and H1972 (Table 1; Fig. 3), which might be attributed to magnetic terrain effect (Baag et al., 1995; Valet and Soler, 1999).

Table 1
Site-mean paleomagnetic directions

Hawaiian flow	*n*/*N*	Dec Obs	Inc Obs	Dec exp.	Inc exp.	*k*	α_{95}
H1950	17/18	10.9	32.9	11.1	37.7	265	2.1
H1955	15/20	10.3	29.7	11.0	37.6	252	2.1
H1960	12/19	13.2	37.0	11.0	37.7	296	2.0
H1972	15/11	9.4	32.1	11.1	37.7	593	1.9
H1977	15/16	14.0	37.1	11.3	37.8	662	1.4
H1982	7/12	13.1	38.0	11.0	37.8	515	1.9
Mean	6	11.8	34.5			480	3.1

Polynesian flow	*n*/*N*	Dec Obs	Inc Obs	*k*	α_{95}
RFA15	9/9	14.1	−40.6	131	4.5
RFA22	6/7	3.7	−25.0	116	6.3

n/*N*, number of samples used in the analysis/total number of samples collected; Dec (Inc) Obs, mean measured declination (inclination); Dec (Inc) exp., declination (inclination) given by the DGRF models; *k*, precision parameter; α_{95}, 95% confidence cone about mean direction of Fisher distribution.

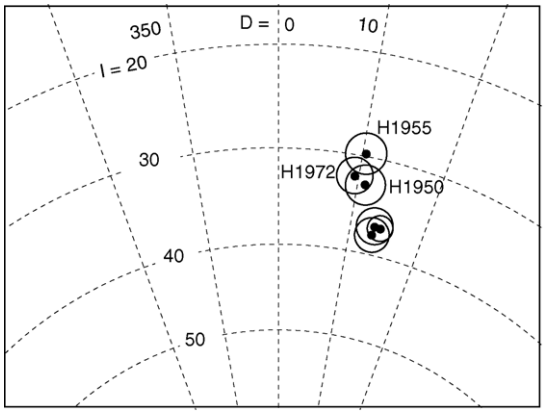

Fig. 3. Stereographic projections of the mean directions after progressive alternating fields demagnetizations for the six lava flows from Hawaii. Three units (H1950, H1955, and H1972) have lower inclinations than the expected 37°.

The paleomagnetic results from Raiatea Island will be discussed elsewhere. Here, we present results from only two lava flows (RFA15 and RFA22; Table 1). The paleomagnetic directions are stable, with no evidence of secondary overprints during the first steps of AF demagnetizations or Thellier experiments.

4. Magnetic properties

4.1. Historical samples from Hawaii

Samples from the six sites exhibit variations of the magnetic properties typical of aerial basaltic lavas (Fig. 4). Flow H1977 has the lowest geometric site-mean magnetization intensity (3.1 A/m), while the mean NRM value for flow H1955 is 11.2 A/m. Median demagnetizing fields (MDFs) are usually greater than 20 mT except for samples for flow H1972, which all have MDF values less than 20 mT.

The magnetic mineralogy and the thermal stability of the magnetic minerals were assessed from thermomagnetic experiments performed in air on 26 specimens (Fig. 5). Most of the samples from flows

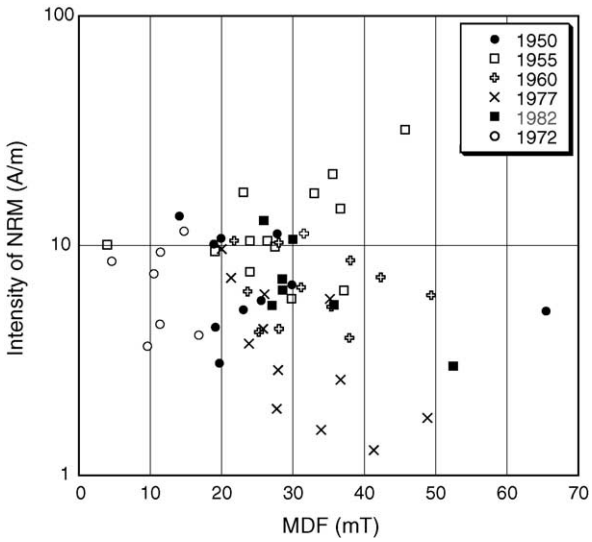

Fig. 4. Mean NRM intensity in Ampere/meter (logarithmic scale) vs. the MDF in milliTesla for all the Hawaiian samples demagnetized by alternating fields.

H1977, H1972, and H1982 have low Curie temperatures. Lavas H1977 and H1982 are vesicular pahoehoe flows and the thermomagnetic behavior is typical of quenched titanomagnetite minerals with little or no exsolution of ilmenite. Samples with low Curie temperatures and reversible Js–*T* curves may give reliable paleointensity results (Mankinen and Champion, 1993). Js–*T* curves for samples from the other flows have higher Curie temperatures, indicating higher degrees of deuteric oxidation during emplacement of the lavas. The ratio of the intensity of the viscous remanent magnetization (VRM) acquired during 10 days of storage in the laboratory field to that of the NRM (Thellier and Thellier, 1944) was measured for 63 samples, and the magnetic viscosity was lower than 3% for all samples. From the observed range in magnetic properties (NRM intensity, MDF, and Curie points), we expect to encounter various types of behavior during the paleointensity experiments, comparable to typical paleointensity studies on non-altered aerial basaltic lavas.

4.2. Samples from Raiatea

The low-field susceptibility versus temperature (*k*–*T*) was measured in air for eight samples from flows RFA15 and RFA22. With one exception, the *k*–*T* curves are reversible with Curie points above 560 °C (Fig. 6), suggesting low Ti contents for the titanomagnetites.

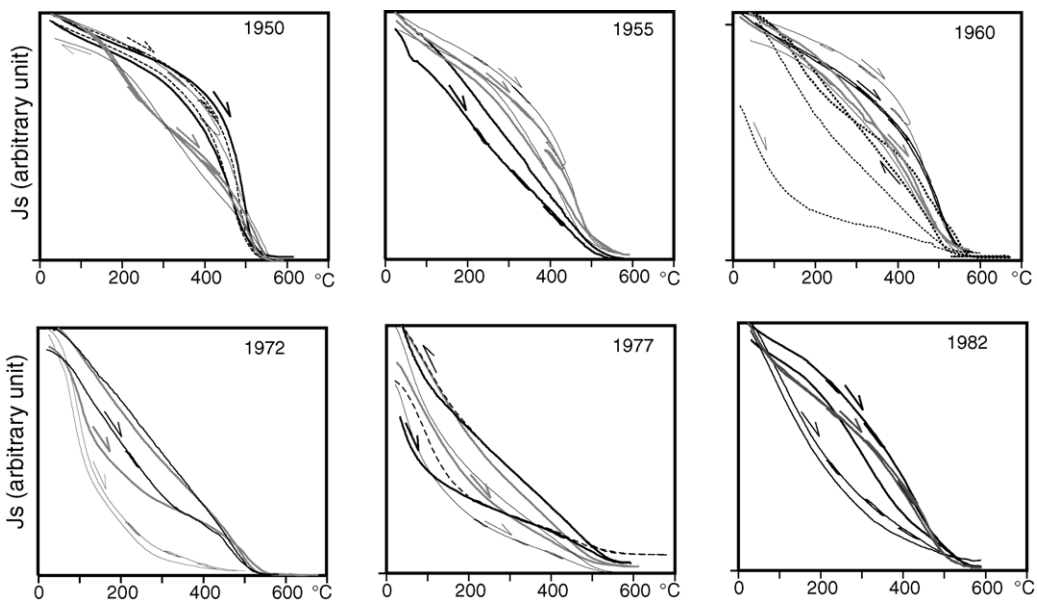

Fig. 5. Strong field thermomagnetic curves for samples from the six flows from Hawaii. Experiments were performed in air; heating and cooling rates were 8 °C/min. Arrows indicate heating or cooling.

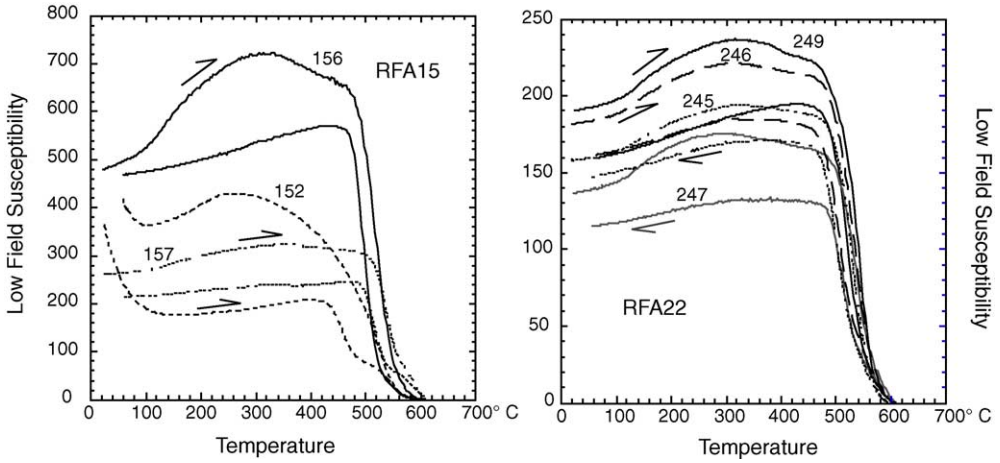

Fig. 6. Variations of the low-field susceptibility vs. temperature for samples from the two lavas from Raiatea Island. Arrows indicate heating or cooling.

Four samples from the flow RFA22 (samples RFA22246, 22245, 22249, and 22252), which presumable carry TRM, were measured for decay of the remanence after one cooling cycle to liquid nitrogen temperature (77 K) and reheating to room temperature in zero field. The NRM intensity decayed between 4 and 6%. For stoichiometric magnetite, low-temperature decay of the magnetization decreases with decreasing grain size and is essentially absent for single-domain particles (e.g., Merrill, 1970; Levi, 1977; Levi and Merrill, 1978). Levi and Merrill (1978) showed that low-temperature cycles to below magnetite's isotropic temperature (130 K) are a very consistent indicator for domain structure in pure magnetite. They reported that for some MD grains carrying TRM, the decay after one low-temperature cycle can be 40%. However, even modest concentrations of titanium on the order of a few percent can suppress the Verwey transition.

The NRMs of all samples from flow RFA22 have MDF values greater than 40 mT. For flow RFA15, the MDFs of the NRMs are lower, with values about 30 mT for four samples and 10 mT for the remaining three. These MDF values together with the small decay during low temperature cycling are in agreement with the hysteresis parameters (to be introduced later). These results suggest that MD particles make only a relatively minor contribution to the NRM of these Raiatea Island samples.

5. Paleointensity data

5.1. Historical lavas from Hawaii

We conducted Thellier experiments on 43 samples from the six historical lava flows from Hawaii. Examples of NRM–TRM diagrams and orthogonal vector projection plots of the paleomagnetic directions are shown in Fig. 7. Samples H1955-03B, H1950-03D, and H1982-01B have ideal behavior during the Thellier experiment with almost all the points aligned on a straight line with successful pTRM checks. About 65% of the samples have this behavior. Increase or decrease of the TRM capacity is also observed (Fig. 7; sample H1972-01A, at 490 °C). Only one sample (from flow H1977) had an entirely unreliable NRM–TRM diagram, characterized by CRM acquisition for temperatures between 360 and 490 °C; the CRM was demagnetized at about 500 °C. The results from this sample were rejected. For all other samples, it was possible to interpret the NRM–TRM plot in the classical way; that is, a temperature interval that includes at least five points distributed on a straight line and representing more than 15% of the original NRM intensity (Coe, 1967) with successful pTRM checks.

The expected field strengths are between 36.2 and 35.5 μT, consistent with the 1950, 1955, 1970, 1975, and 1980 DGRF models.

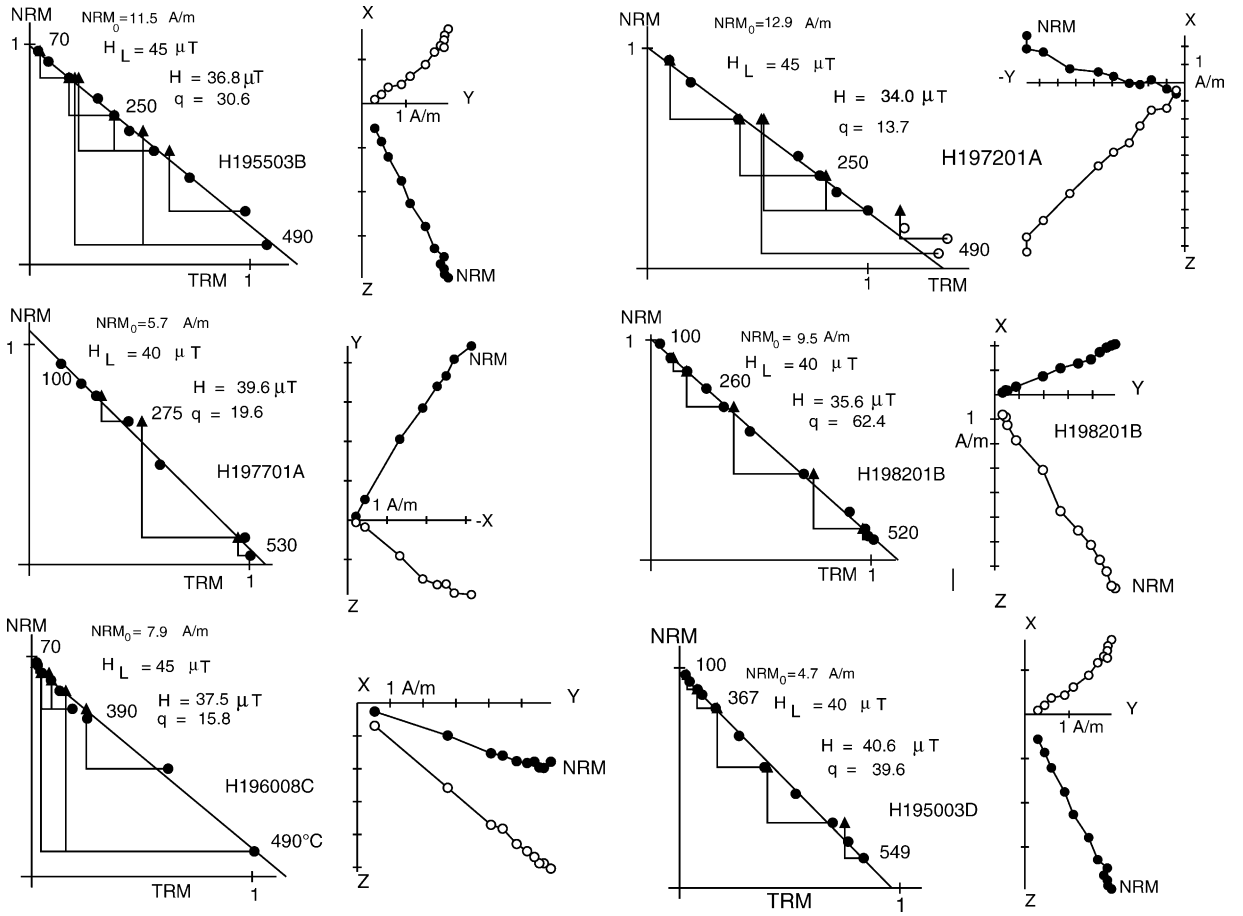

Fig. 7. Examples of NRM–TRM diagrams for samples from Hawaiian flows H1955, H1972, H1982, H1960, H1950, and H1977 and corresponding orthogonal vector projections of the remanence directions in sample coordinates. Filled (open) circles are projections onto the horizontal (vertical) plane. Experiments were performed in vacuum. Diagrams are normalized to the initial NRM (NRM_0). H_L, intensity of the laboratory field in microTesla; H, paleointensity determined; q, quality factor (Coe et al., 1978); triangles, pTRM checks. Temperature steps are in degree Celsius. Closed circles on the NRM–TRM diagrams are data used for the paleointensity calculations.

5.2. Gauss-age lavas from Raiatea Island

We studied nine samples from two Gauss-age flows on Raiatea Island (RFA15 and RFA22) with clear examples of non-linear concave-up behavior (Fig. 8a). Two samples (RFA22245B and RFA15158B) are only mildly non-linear and seem to give reliable paleointensity results (Fig. 8b). On the other hand, three samples from flow RFA22 (RFA22249B, RFA22251B, and RFA22252B) and two from flow RFA15 (RFA15157B and RFA15156B) show strongly concave-up NRM– TRM diagrams, but they have successful pTRM checks to high temperatures and show no CRM acquisition during the Thellier experiment (Fig. 8a).

6. Interpretation of NRM–TRM diagrams

The results from Raiatea Island illustrate the difficulties in interpreting paleointensity data. Completely different paleointensities would be obtained, depending on which line segment is chosen. Variations of the calculated paleointensities on increasing the NRM fraction are shown in Fig. 8c for five samples. It is evident that using smaller NRM fractions from the

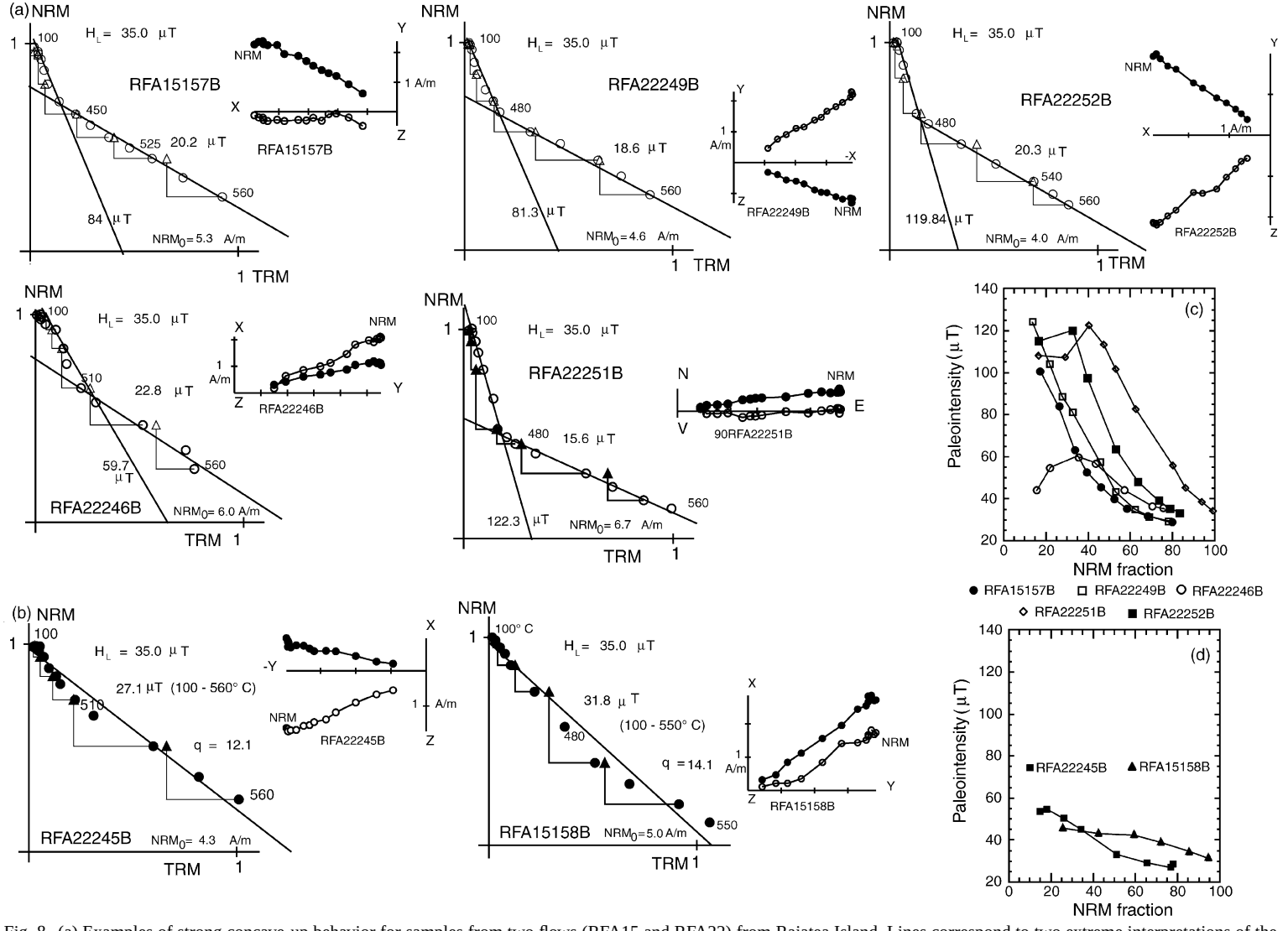

Fig. 8. (a) Examples of strong concave-up behavior for samples from two flows (RFA15 and RFA22) from Raiatea Island. Lines correspond to two extreme interpretations of the NRM–TRM diagram. (b) Two samples from these flows, which are interpreted to give a single paleointensity value (RFA151578B and RFA2225B). Solid circles are points used for the computation of the paleointensity. The corresponding orthogonal vector projections of the directions are shown to the right of each NRM–TRM diagram of (a) and (b); (c) and (d) variations of the paleointensity with the NRM fraction of the linear segments chosen to calculate the field strength.

lower temperature ranges leads to higher paleointensities. When the NRM fractions are extended, all samples give paleointensities approaching 30 μT, similar to values for samples RAF22245B and RFA15158B (Fig. 8d).

Although the curvature is significantly less pronounced in samples from the historical lava flows from Hawaii than for some of the Raiatea samples, several Hawaiian samples show significant concave-up behavior.

To establish guidelines for interpreting the NRM–TRM diagrams, we will further examine the Hawaiian data for which the geomagnetic paleointensities are known.

6.1. A multispecimen approach

For each lava flow, a single Arai diagram (Fig. 9) was constructed using NRM–TRM data for all samples from that unit. TRM values produced in different laboratory fields were renormalized to a field intensity of 37.5 μT, assuming linear TRM acquisition. Each Arai diagram in Fig. 9 includes data from all specimens of a given flow, and each sample was assigned its own symbol. For example, all the NRM–TRM data for the flow H1955 are well distributed on a straight line. The slope of this line is 0.97, calculated by a simple linear fit, using least squares analysis, and the correlation coefficient is 0.99. The resulting paleointensity value is 36.3 μT, very close to the expected value. In most cases, the points that clearly deviate from the general trend correspond to samples with poor pTRM checks, indicating magnetic evolution during heating. These points are indicated by squares in Fig. 9. If these data are rejected, the overall paleointensity for each flow is in good agreement with the expected value. The largest discrepancy is for the H1960 flow. This method of displaying the data is very useful for assessing the quality and consistency of the data at a site level, when secondary overprints can be largely neglected.

6.2. Effect of the NRM fraction

To check if a reliable paleointensity estimate can be obtained from lower unblocking temperatures of our samples, we calculated the paleointensities using dif-

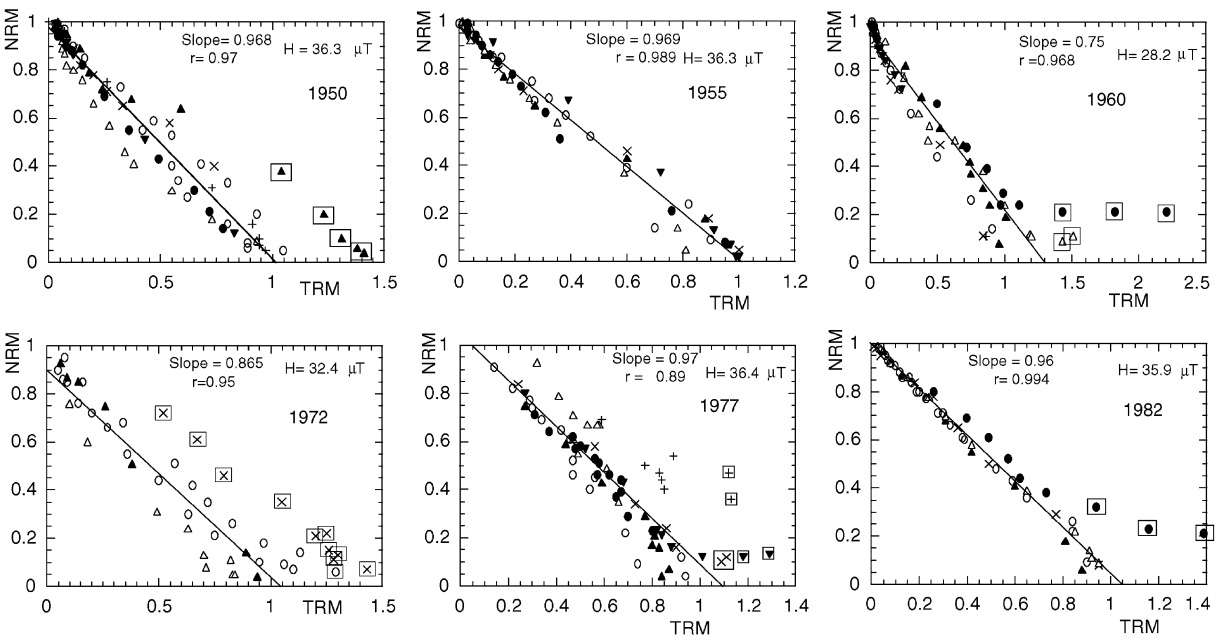

Fig. 9. Composite NRM–TRM diagrams. Each panel shows the behavior of all samples from the same volcanic unit. TRM values produced in different laboratory fields were normalized to a common field intensity of 37.5 μT. In each composite Arai diagram, each symbol represents a particular sample. Data within squares deviate significantly from the trend and were rejected. Also shown are the slopes of the best lines through the data, values of the coefficients of linear correlation (r), and the calculated paleointensities.

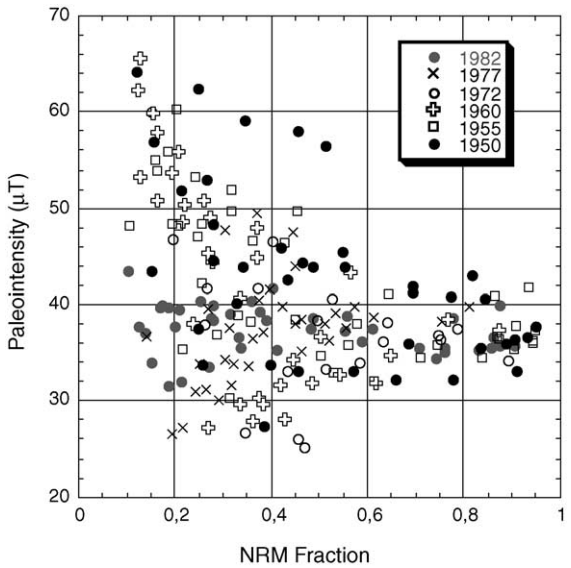

Fig. 10. Paleointensities for the 43 measured samples from the Hawaiian lavas vs. the percentage of the NRM (*f*) used for the calculations.

ferent NRM fractions. We used only linear segments with at least three points. We required that within any chosen temperature interval the pTRM checks had to be successful with no evidence for CRM acquisition. Two hundred and four determinations of field strength versus NRM fraction are shown on the Fig. 10. Because our samples carry almost no secondary overprints, the data in Fig. 10 reflect the primary remanence. It is apparent that the scatter in the paleointensity estimates increases significantly for lower NRM fractions, when only the first few steps of the Thellier experiments are used. For NRM fractions less than 20%, field strengths range between 66 and 26 μT, while for NRM fractions greater than 80% the paleointensities are between 44 and 33 μT.

We calculated the arithmetic mean paleointensity per flow using three different values of the NRM fraction (*f*): less then 20%, between 20 and 40%, and between 40 and 50%. For each *f*-range, only one determination per sample was used, and in each *f*-interval we retained the paleointensity value corresponding to the lowest value of the NRM fraction, and satisfying the conditions of linearity defined by a minimum of three points, successful pTRM checks, and no evidence for CRM. Sometimes it was not possible to do these

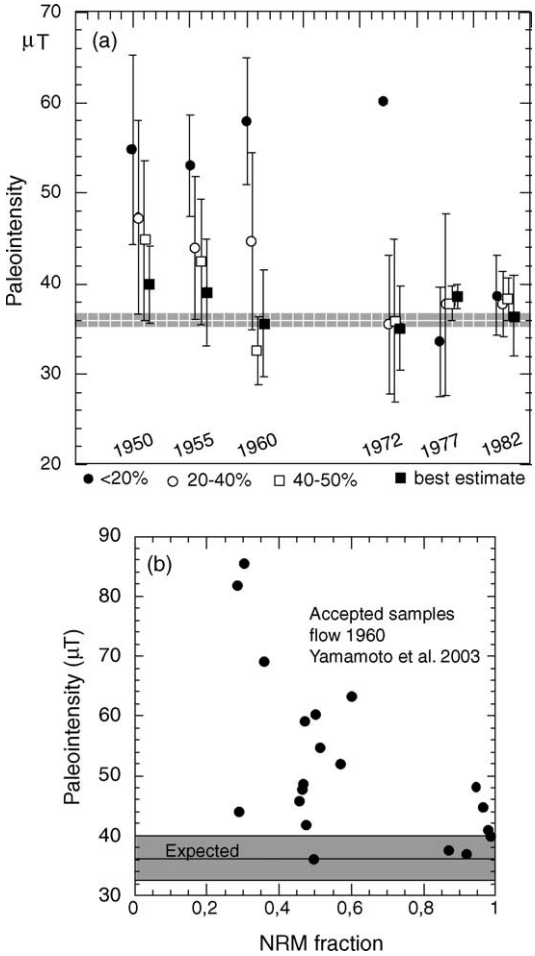

Fig. 11. (a) Arithmetic mean paleointensity per flow and standard error of the mean, using three different values of the NRM fraction: less then 20%, between 20 and 40%, and between 40 and 50%. Solid squares: weighted mean paleointensity; H_w, calculated using the "best estimate" analysis (see text). Expected value of the field is about 36 μT. (b) Paleointensity values of Yamamoto et al. (2003) for samples from the 1960 Hawaiian flow vs. the NRM fraction used for the calculations.

calculations for all three *f*-ranges of each sample, because of their different blocking temperature distributions (Table 2; Fig. 11a).

The mean intensity per flow is more scattered when less than 40–50% of the NRM is used, and sometimes it is very different from the expected field strength. However, the observed scatter could be partly explained by the fewer number of samples used for the calculations in the lower *f*-intervals (see Table 2).

Table 2
Paleointensity results for different NRM fractions

Sample	T_{min}–T_{max}	N	f	H	q	T_{min}–T_{max}	N	f	H	q	T_{min}–T_{max}	N	f	H	q
H195001A											100–240	3	0.43	42.5	19.1
H195003D	100–370	5	0.15	43.5	2.4	100–430	6	0.27	44.7	9.1	100–470	7	0.42	46	20.3
H195005A						100–400	6	0.25	33.7	2.2	100–480	8	0.45	33.2	14.7
H195007A						100–350	5	0.26	53.1	2.4					
H195009B						100–430	6	0.25	37.6	1.7					
H195010B	70–250	5	0.15	56.9	1.2	70–300	6	0.21	51.9	2.4					
H195011A						100–400	7	0.25	62.6	1.7	100–460	9	0.45	58.0	8.0
H195012B	100–350	5	0.12	64.2	1.5						100–480	6	0.46	44.3	4.3
1950			54.8 ± 10.5					47.3 ± 10.7					44.8 ± 8.8		
H195503A						70–200	4	0.22	35.3	3.12	70–350	7	0.45	38.5	16.3
H195504B	100–350	6	0.16	54.9	1.3	100–430	8	0.25	47	3.6	100–490	10	0.45	49.8	10.3
H195505A	100–400	6	0.18	55.9	1.1	100–440	7	0.24	53.2	2.4	100–500	9	0.43	46.4	7.7
H195507A	100–400	6	0.20	48.4	1.7	100–440	7	0.25	42.2	2.6	100–500	9	0.43	46.4	7.7
H195508B	100–300	4	0.16	53.8	1.6	100–370	5	0.25	48.3	3.3					
H195509B						150–440	6	0.31	30.4	1.6					
H195510A	100–350	5	0.14	44.5	2.0	100–480	6	0.32	44.1	12.9					
H195513A	100–310	4	0.20	60.3	1.5	100–370	5	0.32	51.8	3.1					
1955			53 ± 5.6					44 ± 7.9					42.4 ± 6.9		
H196001A	100–310	4	0.16	50.8	2.1	100–370	5	0.22	50.3	5.9					
H196002B	75–325	11	0.13	65.6	1.6	75–400	13	0.21	48.6	2.5					
H196003B	100–400	6	0.12	62.2	3	100–500	9	0.27	49.0	5.2					
H196007A						100–235	3	0.28	44.3	2.5	100–400	6	0.44	34.3	1.7
H196008C	70–300	5	0.13	53.3	1.1	70–390	7	0.21	55.9	3.4	70–440	8	0.5	36.6	4.3
H196010A						100–200	3	0.27	27.1	1.5	100–400	7	0.43	28.0	3.1
H196011A						70–150	3	0.24	38	37.2					
1960			58.0 ± 7.0					44.7 ± 9.5					32.6 ± 3.7		
H197201A						70–150	3	0.26	37.9	1.7	70–200	4	0.43	33.2	4.2
H197207A	100–260	4	0.15	60.2	1.2	100–350	6	0.26	41.7	2.2	100–430	8	0.49	38.5	8.6
H197207B											100–350	5	0.4	46.6	2.0
H197211B															
H197215B						150–390	4	0.34	26.8	1.5	150–440	5	0.47	25.2	3.8
1972					60.2			35.5 ± 7.7					35.9 ± 9.0		
H197710B	75–200	6	0.19	26.6	1.0	75–225	7	0.22	27.1	1.7	75–450	14	0.46	38.4	5.4
H197704B						100–200	3	0.35	33.7	9.5					
H197701A	100–200	3	0.14	36.6	1.3	100–275	4	0.25	33.9	4.1	100–350	5	0.42	39.7	4.5
H197702A						70–150	3	0.31	37.5	3.5	70–250	4	0.46	35.1	6.9
H197706A											100–235	3	0.45	38.0	1.6
H197713B						70–490		0.39	58.8	1.6					
H197713A	100–240	3	0.2	37.6	1.2	100–300	4	0.22	39.6	1.5					
H197714B						70–250	4	0.21	33.1	1.4					
1977			33.6 ± 6.0					$37.7 \pm 10.$					37.8 ± 1.9		
H198203A	100–200										100–200	3	0.41	35.3	6.5
H198203B	70–200	4	0.17	39.9	1.3	70–250	5	0.25	40.5	4.2	70–350	7	0.48	38.7	16.5
H198204A	70–250	4	0.15	34.0	1.0	70–300	5	0.21	32.0	3.2	70–390	7	0.48	37.6	9.4
H198202B	70–250	4	0.19	39.8	1.7	70–300	5	0.27	40.1	5.7	70–350	6	0.40	41.7	11.5
H198206C	75–175	5	0.1	43.6	1.8	75–275	9	0.21	39.5	40	100–350	12	0.40	39.3	16.9
H198201B	100–250	4	0.2	37.8	2.0	100–300	5	0.28	38.4	5.8	100–350	6	0.39	38.4	14.4
1982			39.0 ± 3.5					38.1 ± 3.5					38.2 ± 2.1		

T_{min}–T_{max}, temperature interval used to determine the paleointensity; f, NRM fraction; N, number of points in the temperature interval; H, paleointensity estimate for individual specimen (μT); q, quality factor.

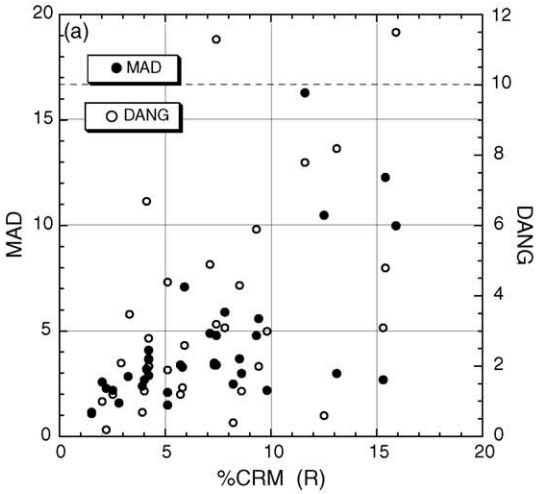
(a)
MAD
DANG
%CRM (R)

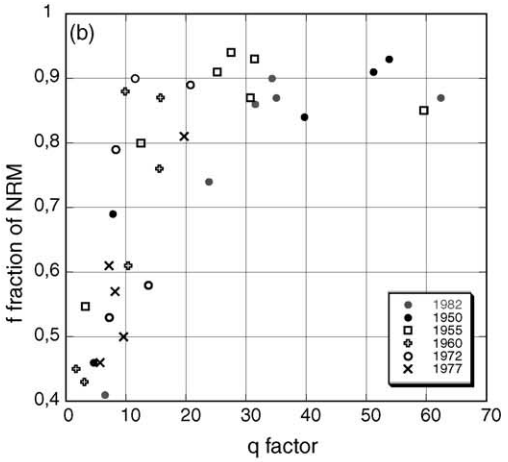
(b)
f fraction of NRM
q factor
1982
1950
1955
1960
1972
1977

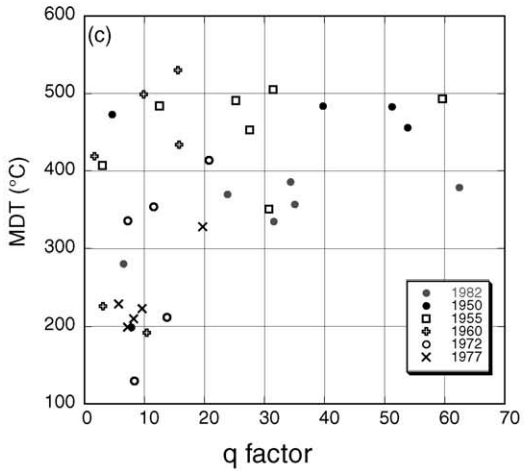
(c)
MDT (°C)
q factor
1982
1950
1955
1960
1972
1977

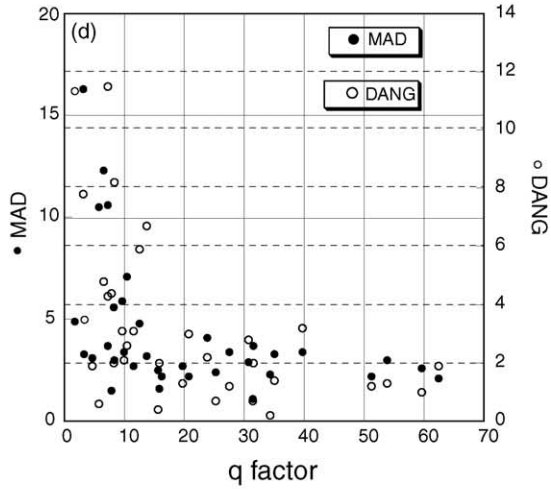
(d)
MAD
DANG
q factor

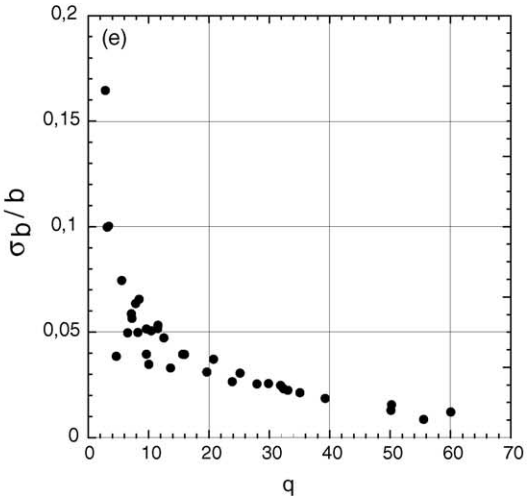
(e)
σb / b
q

Results presented in Figs. 10 and 11a indicate that paleointensity determinations using smaller fractions of the NRM intensity, typically less than 40%, are often in error and are usually biased to higher paleointensity values. In older and even recent publications, paleointensity data are frequently restricted to lower temperature intervals, often comprising less then 25% of the NRM intensity. Therefore, caution should be exercised before interpreting the absolute paleointensities from such studies, as part of the observed scatter in the results could be explained by this effect.

6.3. The best estimate

In this case, we determined the paleointensity following the usual analysis: at least five points must be distributed on a straight line in a temperature interval T_{min}–T_{max}. The highest temperature (T_{max}) is the temperature where significant modifications of the magnetic mineralogy are observed, as detected by changes in pTRM acquisition or by the growth of CRM. We consider that a pTRM check is successful when it deviates from the corresponding double-heating data point by less than 10% of the total laboratory TRM acquired by the sample. This criterion is very similar to that recently proposed by Selkin and Tauxe (2000) and Laj et al. (2002). Following Chauvin et al. (1991), the *R*-factor, defined by Coe et al. (1984), was calculated for each sample. This factor is an estimate of the maximum potential error to the paleointensity caused by CRM acquisition during the Thellier experiment in percent of the applied field. We fixed the acceptable error limits at no more than 15%. More recently, Selkin and Tauxe (2000) and Tauxe and Staudigel (2004) suggested using two angles: maximum angular deviation (MAD, which is a measure of the scatter in NRM directions) and deviation angle (DANG, which tests whether the component selected is actually trending to the origin) to characterize the stability of the NRM vector used in the paleointensity experiment. The parameters *R*, MAD, and DANG give almost the same information (Fig. 12a; Table 3).

Following Chauvin et al. (2000), the temperature interval chosen for calculating the best estimates of the paleointensity was chosen to represent at least 40% of the original NRM intensity. The results are presented in Table 3 and Fig. 11a. The average paleointensity was calculated using the weighting factor *w*, defined by Prévot et al. (1985). This weighting factor depends on the quality factor *q* (Coe et al., 1978). The *q*-factor is especially low when low NRM fractions are used (Fig. 12b). Also, paleointensity determinations for samples with median demagnetizing temperatures (MDTs) lower than 300 °C have low quality factors (Fig. 12c). Samples with large MAD or DANG usually have low quality factors (Fig. 12d), but there are a few samples with low quality factor q, which have low MAD and DANG values. There is a correlation (Fig. 12e) between the *q*-factor and the ratio σ_b/b (σ_b is the standard error of the slope and *b* is the least squares slope). The data shown in Fig. 12 indicate that the quality factor *q* remains valuable for weighting paleointensity determinations.

When the weighted mean paleointensities (H_w) are compared to those expected from the DGRF models, the typical deviations are less than 10%. Also, discrepancies between weighted field strength and paleointensities determined by the multispecimen approach are typically less than 10%, except for the flow H1960 (Table 3).

We consider that H_w, our best estimate value, is the most accurate and representative paleointensity for each cooling unit, because it includes data from every sample in proportion to its *q* factor. To compare the quality of paleointensity values for different units, we propose a new factor, $Q = N\langle q\rangle$, for the samples with useful paleointensity data for which a *q* was calculated ($\langle q\rangle$ is the arithmetic mean per flow of *q* values, *N* is the total number of samples used to calculate the paleointensity). *Q*-values are listed in Table 3. This representation of *Q* emphasize the importance of measuring multiple samples from each unit. *Q* for H1960 is not very high which might explain the discrepant results of former studies. To assess the accuracy of the field estimate within a flow, Selkin and Tauxe (2000) also propose to calculate the ratio σ/B, where *B* is the field average and σ its standard deviation. According to these authors, values of this ratio should not ex-

Fig. 12. Variations of some parameters obtained on Hawaiian samples (see Table 3). MAD, maximum angle of deviation; DANG, deviation angle (Tauxe and Staudigel, 2004); *f*, NRM fraction; *q*, quality factor (Coe et al., 1978); *R*, percentage of CRM acquired (Coe et al., 1984); σ_b, standard error of the slope; *b*, absolute value of the best fit slope; σ_b/b, uncertainty of the slope; MDT, median destructive temperature.

Table 3
Best estimate paleointensity results

Sample	T_{min}–T_{max}	MDT	H_L	N	f	g	b	sb	σ_b/b	MAD	DANG	R	q	H	$H \pm$ S.D.	H_w	H_M	Q
H195001A	100–427	199	40	6	0.69	0.73	1.0512	0.0675	0.064	1.5	4.4	5.1	7.8	42.0				
H195003D	100–549	484	40	11	0.84	0.87	1.0160	0.019	0.019	3.4	3.2	7.4	39.7	40.6				
H195005A	100–560	483	40	12	0.91	0.87	0.8271	0.0131	0.016	2.2	1.2	2.5	51.2	33.1				
H195009B	100–549	456	40	11	0.93	0.70	0.9164	0.0119	0.013	3	1.3	8.6	53.8	36.6				
H195012B	100–480	473	40	7	0.46	0.38	1.0231	0.0264	0.026	3.1	1.9	7.1	4.6	44.3	39.3 ± 4.5	37.2	36.3	157
H195503B	100–490	351	45	10	0.87	0.87	0.8147	0.0207	0.025	2.9	2.8	4.2	30.7	36.7				
H195504B	100–540	484	40	11	0.80	0.74	1.0326	0.0494	0.048	4.8	5.9	9.3	12.5	41.3				
H195505A	100–560	505	40	12	0.93	0.84	1.0462	0.0258	0.025	1.1	0.7	1.5	31.4	41.8				
H195507A	100–549	491	40	12	0.91	0.85	0.9429	0.0290	0.031	2.4	0.7	3.9	25.2	37.7				
H195509B	100–531	453	30	10	0.94	0.77	1.2115	0.0314	0.026	3.4	1.2	5.7	27.5	36.3				
H195510A	100–530	493	40	7	0.85	0.56	1.1443	0.0098	0.009	2.6	1.0	2.0	59.6	45.7				
H195513A	100–427	407	40	6	0.56	0.68	0.8910	0.0950	0.11	2.8	3.5	3.4	3.6	35.6	39.3 ± 3.7 39.9 ± 3.7[a]	41.1 41.2[a]	36.3	190.4
H196002A	100–530	499	40	7	0.88	0.40	0.9460	0.0335	0.035	3.4	2.1	7.3	9.9	37.8				
H196003B	100–549	530	40	12	0.76	0.81	0.9581	0.0384	0.04	2.5	0.4	8.2	15.6	38.3				
H196007A	100–437	419	30	7	0.58	0.80	0.935	0.1540	0.16	4.8	11.3	7.4	2.8	28.1				
H196008C	70–490	434	45	9	0.87	0.71	0.8330	0.0325	0.039	1.6	2.0	2.8	15.8	37.5				
H196010A	100–350	226	40	6	0.43	0.73	0.7013	0.0696	0.099	16.3	7.8	11.6	3.1	28.0				
H196011A	70–440	192	45	9	0.61	0.86	0.7094	0.0360	0.051	7.1	2.6	5.9	10.4	31.9	33.6 ± 4.9 34.7 ± 4.6[a]	35.5 36.0[a]	28.2	57.6
H197201A	70–300	212	45	6	0.58	0.76	0.7543	0.0247	0.033	3.2	6.7	4.1	13.7	34.0				
H197207A	100–520	414	40	11	0.89	0.87	0.8578	0.0323	0.038	2.2	3.0	9.8	20.7	34.3				
H197207B	100–530	354	40	7	0.90	0.68	0.9168	0.0494	0.054	2.7	3.1	15.3	11.5	36.7				
H197211B	100–350	130	45	6	0.79	0.70	0.8369	0.0554	0.066	3.0	8.2	13.1	8.3	37.6				
H197215B	150–518	336	30	8	0.53	0.78	0.9076	0.0504	0.056	10.6	11.5	15.9	7.2	28	34.1 ± 3.7	34.5	32.4	61.5
H197701A	100–530	328	40	7	0.81	0.75	0.8121	0.0599	0.074	2.7	1.3	4.0	19.7	39.7				
H197702A	70–300	223	45	5	0.50	0.72	0.8071	0.0319	0.04	5.9	3.1	7.8	9.6	36.3				
H197704B	100–350	210	40	6	0.57	0.72	0.9985	0.0501	0.05	5.6	2.0	9.4	8.2	39.9				
H197706A	100–350	199	30	5	0.61	0.68	1.2904	0.0758	0.059	3.7	4.3	8.5	7.2	38.8				
H197710B	70–450	229	40	14	0.46	0.89	0.9642	0.0722	0.075	10.5	0.6	12.5	5.7	38.4	38.6 ± 1.4	38.7	36.4	50.4
H198201B	100–520	379	40	11	0.87	0.85	0.8924	0.0111	0.012	2.1	1.9	5.1	62.4	35.7				
H198202B	70–490	357	45	9	0.87	0.84	0.8872	0.0187	0.021	3.3	1.4	5.8	35.0	39.9				
H198203B	70–490	335	45	10	0.86	0.87	0.8147	0.0190	0.023	3.7	2.0	4.2	31.5	36.6				
H198203A	100–350	281	40	6	0.41	0.78	0.8827	0.0440	0.05	12.3	4.8	15.4	6.5	35.5				
H198204A	70–490	386	45	9	0.90	0.82	0.7972	0.0180	0.023	2.3	0.2	2.2	34.3	35.9				
H198206C	70–450	370	40	14	0.74	0.84	0.8615	0.0225	0.026	4.1	2.2	4.2	23.8	34.4	36.3 ± 1.9	36.6	35.9	193.2
RFA22252B	100–560	510	35	13	0.836	0.878	0.947	0.091	0.096	3.3	3.3	9.2	7.6	33.1				
RFA22249B	100–560	521	35	14	0.782	0.888	0.834	0.073	0.088	3.5	2.6	5.9	7.9	29.2				
RFA22246B	100–560	532	35	13	0.762	0.856	0.990	0.070	0.071	3.5	4.2	8.7	9.2	34.7				
RFA22245B	100–560	536	35	14	0.767	0.841	0.775	0.041	0.053	3.7	2.2	4.3	12.1	27.1	31.0 ± 3.5	30.8	30.8	36.8
RFA15157B	100–540	519	35	12	0.584	0.886	1.007	0.093	0.092	5.2	3.4	6.6	5.6	35.2				
RFA15158B	100–550	483	35	12	0.945	0.864	0.910	0.053	0.058	4.3	3.4	7.0	14.1	31.9	33.5 ± 2.3	32.8	31.1	19.6

T_{min}–T_{max}, temperature interval used to determine the paleointensity (°C); N, number of points in the temperature interval; H_L, laboratory field (μT); f, NRM fraction; q, quality factor; H, paleointensity estimate for individual specimens (μT); $H \pm$ S.D., unweighted mean paleointensity of individual lava flows (μT) plus or minus its standard deviation; H_w, weighted mean paleointensty (μT); H_M, multispecimen (see text μT); b, absolute value of the slope; σ_b, standard error on the slope; R, percentage of CRM; MAD, DANG, maximum angle of deviation and deviation angle.

[a] Site-mean paleointensity calculated excluding samples with $\sigma_b/b > 0.1$.

ceed 0.25 for the field estimate to be considered reliable and accurate. This criterion does not however take into account the quality of individual paleointensities. It is easy to imagine a case with few determinations of poor reliabilities with low individual q with similar paleointensities values and thus a low ratio of σ/B. The Q factor will reflect the reliability at the site level.

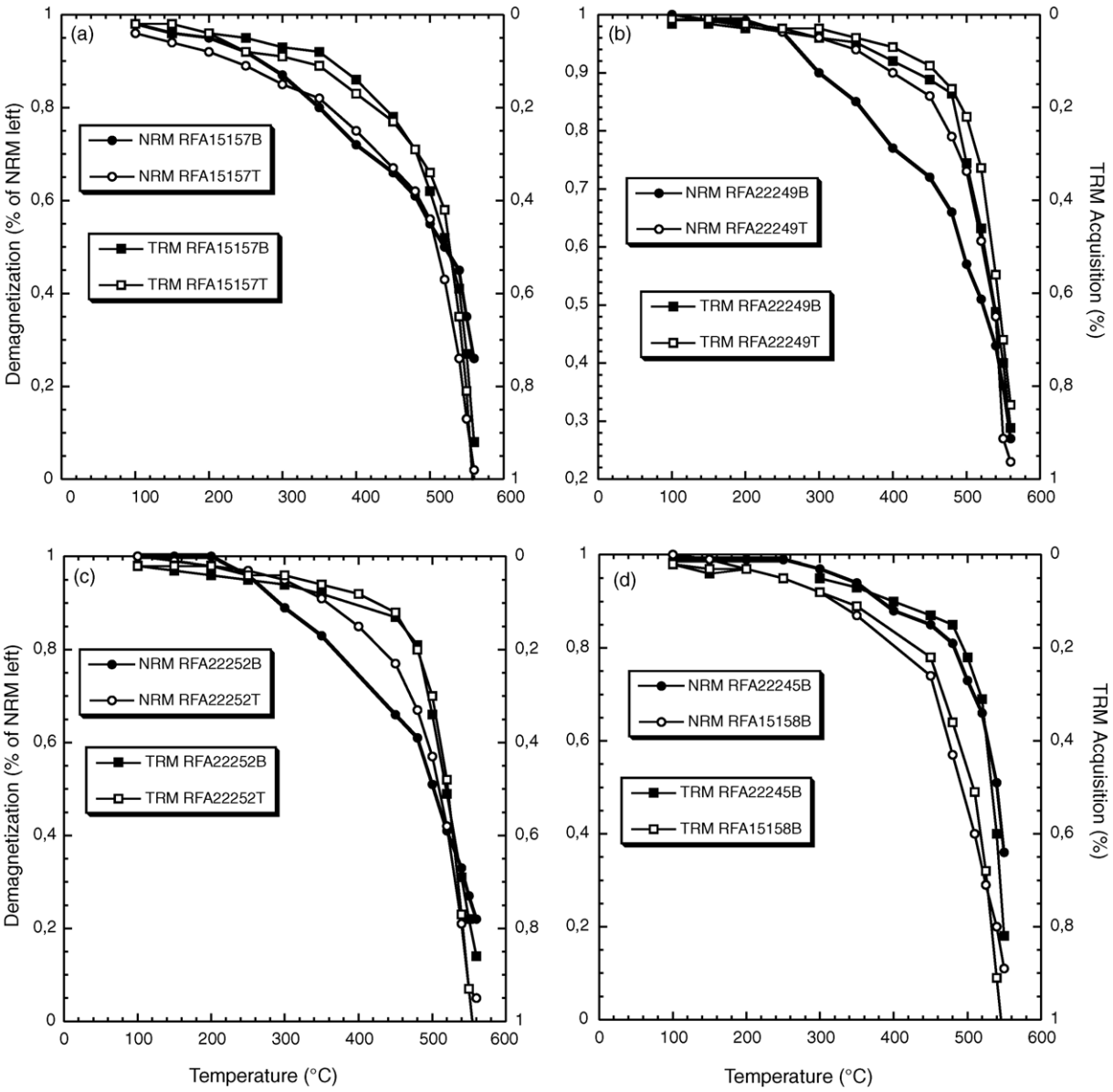

Fig. 13. Unblocking and blocking temperatures for samples from Raiatea Island from Fig. 8a and Fig. 14. Values for each sample are normalized to the initial NRM (NRM_0).

7. Discussion

Three of the six Hawaiian flows (H1950, H1955, and H1960) have mean paleointensity values which depend strongly on the NRM fraction (Fig. 11a; Table 2), and restricting the analyses to the lower temperature points on the NRM–TRM diagrams leads preferentially to higher mean paleofield strengths. Samples from flows H1950, H1955, and H1960 are more oxidized than the other three flows, and one of the reason for concave-up behavior seems to be related to a significant unblocking of NRM in the temperature range 200–450 °C for samples with MDT above 400 °C.

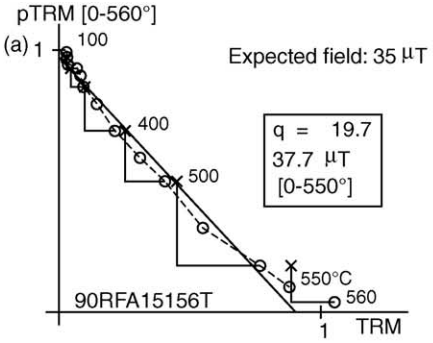
pTRM [0-560°]
(a)
Expected field: 35 μT
q = 19.7
37.7 μT
[0-550°]
90RFA15156T
TRM

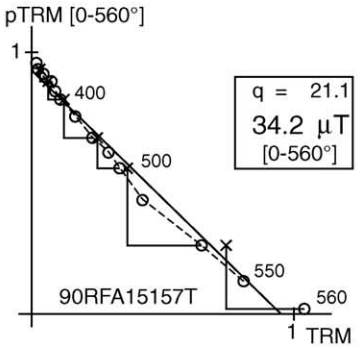
pTRM [0-560°]
q = 21.1
34.2 μT
[0-560°]
90RFA15157T
TRM

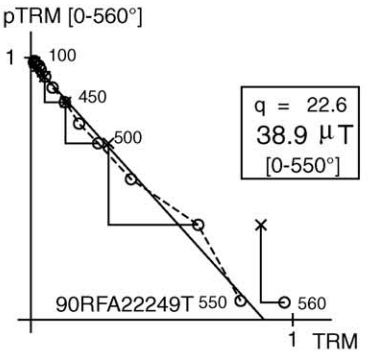
pTRM [0-560°]
q = 22.6
38.9 μT
[0-550°]
90RFA22249T
TRM

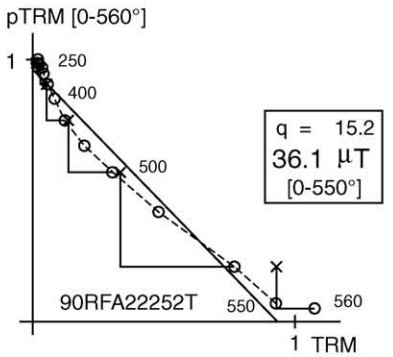
pTRM [0-560°]
q = 15.2
36.1 μT
[0-550°]
90RFA22252T
TRM

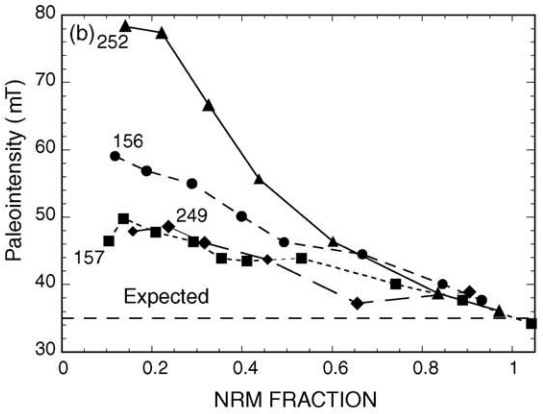
(b)
Paleointensity (mT)
Expected
NRM FRACTION


RFA1516T
RFA22252T
RFA15157T
RFA22249T

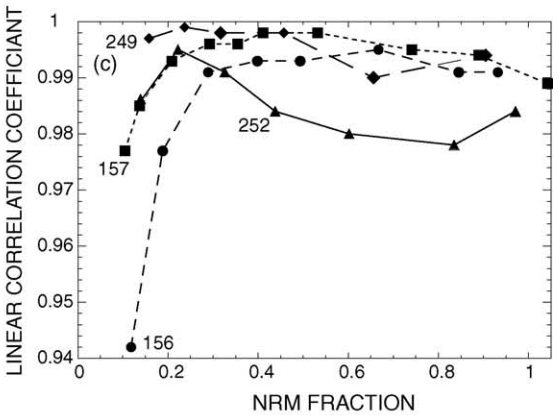
(c)
LINEAR CORRELATION COEFFICIANT
NRM FRACTION

Several studies using both the Shaw and Thellier methods, including microwave heating, have reported discrepant values for the Hawaiian H1960 lava (Abokhodair, 1977; Tanaka and Kono, 1991; Tsunakawa and Shaw, 1994; Hill and Shaw, 2000; Yamamoto et al., 2003). Typically the paleointensity estimates are 11–35% higher than the International Geomagnetic Reference Field (IGRF) value of 36.2 μT. Yamamoto et al. (2003) studied the H1960 flow, and they classified their samples in three groups (A, B, and C) according to increasing oxidation state. Higher than expected paleointensities were observed for group B samples, while the least oxidized samples (group A) and samples with highest deuteric oxidation (class C) gave more accurate values. Group C samples had the most linear NRM–TRM diagrams over the full temperature range. Yamamoto et al. (2003) attributed the high paleointensity values observed on group B samples to the acquisition of thermochemical remanent magnetization (TCRM) during the natural cooling of this lava with continuous oxidation occurring below the Curie temperature. If true, this kind of samples would be unsuitable for paleointensity experiments. However, TCRM may not be the only explanation for the erroneous paleointensities previously obtained for the Hawaii 1960 flow. Most high paleointensities found by Yamamoto et al. (2003) correspond also to low NRM fraction (Fig. 11b).

Our results on flows H1950, H1955, and H1960 (see Figs. 9 and 10) show that taking the best-fitting line through all points with successful pTRM checks and no CRM acquisition, leads to more accurate paleointensity results than trying to define the "most straight" line. Hill and Shaw (2000) reached the same conclusions using microwave heating. However, their experiments did not include pTRM checks.

In order to explain the higher than expected paleointensities (Fig. 11a), we consider two physical processes that can lead to overestimates of paleointensity determinations with no recourse to chemical or mineralogical alterations. These processes arise from the much slower initial cooling of the rock in nature than heating/cooling cycles in the laboratory during Thellier experiments. First, cooling-rate-dependence in SD particles will cause higher TRM intensity during slower cooling (Dodson and McClelland, 1980; Fox and Aitkin, 1980). Second, high temperature VRM during the slower initial cooling in nature would also enhance the NRM. The VRM contribution in any temperature interval will be greater during the initial cooling than during subsequent pTRM steps in the same temperature interval during Thellier experiments. Both mechanisms act in the same direction to increase the TRM. The magnitude and temperature distribution of the VRM will depend on the blocking temperature distribution in the sample. At a particular temperature, during the Thellier experiment, NRM decay will exceed the pTRM production, especially at lower temperatures; this disparity will diminish as the Curie point is approached, producing concave-up NRM–TRM diagrams.

Samples from Raiatea Island have concave-up curvature of their NRM–TRM diagrams more pronounced than the slight curvature observed in samples of historical flows from Hawaii. The decrease of the NRM intensity between 200 and 480 °C is not matched by a corresponding pTRM acquisition. In this temperature range, the unblocking and blocking temperatures are different for these samples (Fig. 13a–c). For the two samples RAF22245B and RFA15158B (Fig. 8b), whose NRM–TRM diagrams are more nearly linear, the blocking and unblocking temperatures are similar (Fig. 13d). The difference between blocking and unblocking temperatures (Fig. 13a–c) might be attributed to: (1) MD or PSD particles, with lower unblocking than blocking temperatures; (2) irreversible chemical changes during heating, transforming magnetic minerals with unblocking temperatures between 200 and 480 °C to a new magnetic phase with higher unblocking temperatures. Such transformations usually leads to CRM acquisition, not observed in the present study.

Fig. 14. (a) NRM–TRM diagrams for samples from Raiatea Island, where the "NRM" was produced in a known laboratory field of 35 μT (see text). The paleointensity listed for each panel is the value obtained using temperature intervals given in the parenthesis. Crosses indicates pTRM checks, q is the quality factor. (b) Variations of the paleointensity versus the NRM fraction included in the linear segments chosen to compute the field strength for the samples shown in (a). (c) Linear correlation coefficients of linear fits for different NRM fractions used for the same samples.

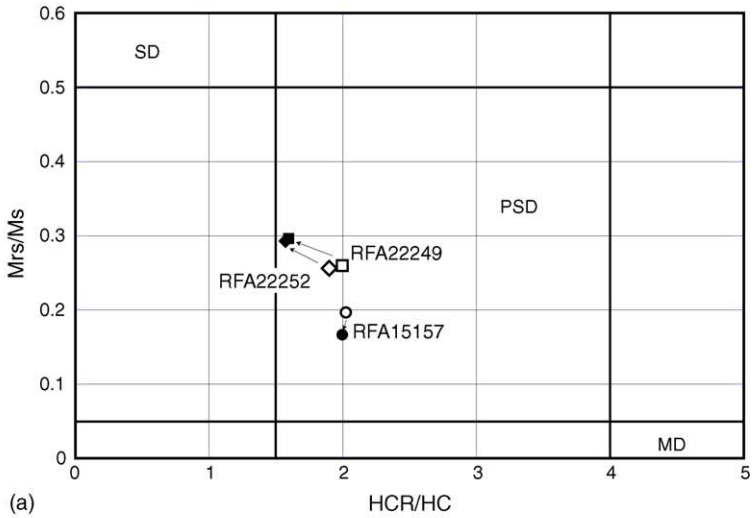
SD
PSD
MD
RFA22249
RFA22252
RFA15157
Mrs/Ms
HCR/HC
(a)

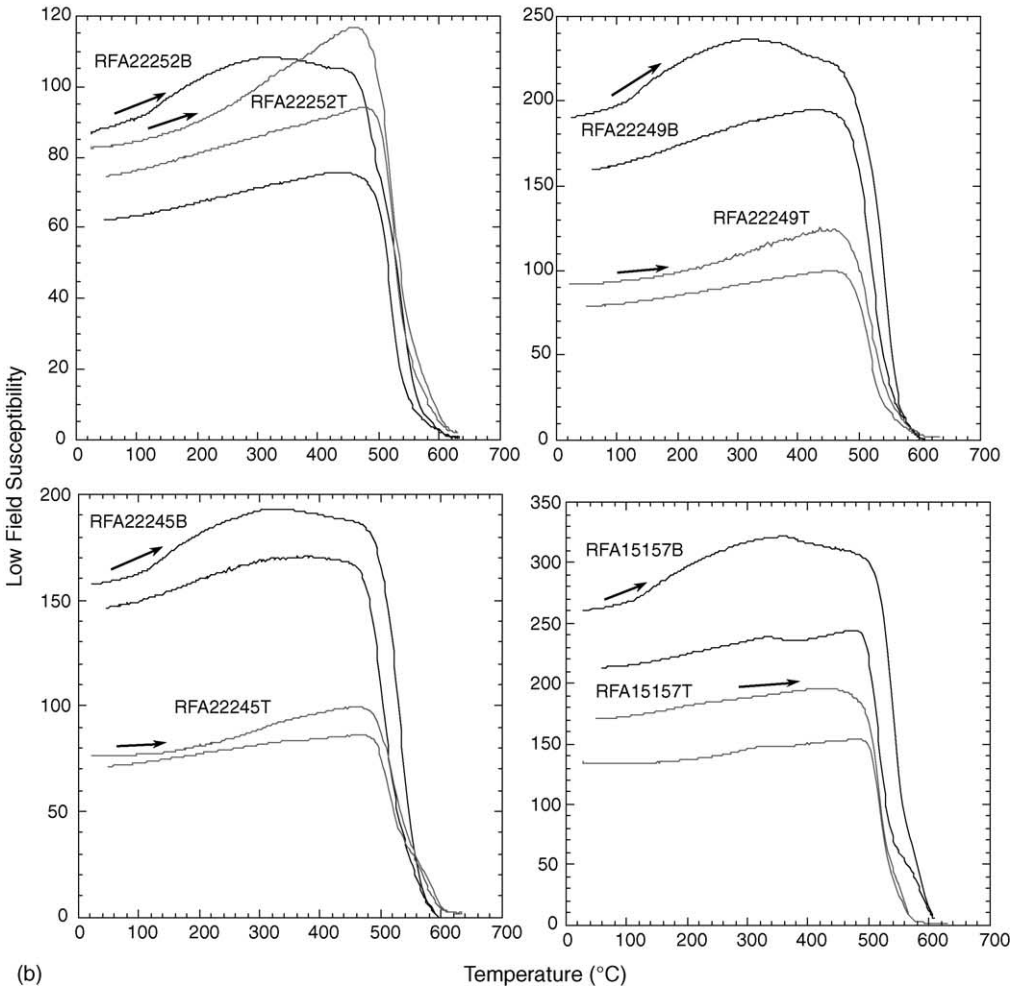
RFA22252B
RFA22252T
RFA22249B
RFA22249T
RFA22245B
RFA22245T
RFA15157B
RFA15157T
Low Field Susceptibility
Temperature (°C)
(b)

Concave-up NRM–TRM plots frequently originate from chemical alterations and increased TRM capacity of the minerals at higher temperatures of the Thellier experiments. However, MD particles can also give rise to reproducible concave-up NRM–TRM diagrams. Levi (1977) demonstrated concave-up Arai diagrams for laboratory-prepared samples with MD magnetite particles, and he noted that for samples exhibiting such behavior "the ratio of the end-points, NRM:TRM, yields the correct (laboratory) intensity". We emphasize, however, that for typical paleointensity studies, where the NRM was produced in an unknown paleofield, it would be a mistake to base the paleointensity determinations on a two point calculation. In both synthesized and natural MD samples, a linear fit to the lower temperature points on Arai diagrams leads to paleointensity overestimates (Shcherbakov and Shcherbakova, 2001). The experimental pTRM tail check of Riisager and Riisager (2001) was introduced in the Coe version of the Thellier method to detect samples where there is failure to fully demagnetize a laboratory pTRM (acquired at a particular temperature step) carried by magnetic grains with blocking temperatures lower than unblocking temperature. In our experiment we observe that the NRM (acquired between Curie and room temperatures) is carried partially by grains with blocking temperatures higher than unblocking temperatures, consistent with the phenomenological theory of TRM of Fabian (2001), where curvature of the Arai plot can be attributed to magnetizations in PSD and MD particles, which are unblocked at temperatures below their blocking temperatures. Therefore, the pTRM tail check will be inefficient in this case (see also Yu et al., 2004).

To further investigate the concave-up behavior of samples from Raiatea Island, we performed a second Thellier experiment on four samples that exhibited concave-up behavior during the initial Thellier experiments. The "NRM" for the second Thellier experiment was the partial-TRM produced by cooling from 560 °C at the end of the first Thellier experiment in a laboratory field of 35 μT, which, of course, is the expected paleointensity.

The curvatures of the NRM–TRM plots of the second Thellier experiments are diminished in comparison to the first experiment (compare Fig. 8a and c with Fig. 14a and b). pTRM checks up to 540 °C are successful and orthogonal plots of the directions indicate no CRM acquisition. While the unblocking temperatures of samples have changed significantly between the first and second Thellier experiments (Fig. 13a–c), the changes in the blocking temperatures are small. The discrepancy between the blocking and unblocking temperatures in the temperature interval 200–480 °C remains, but is much diminished during the second Thellier experiment (Fig. 13a–c)

The second Thellier experiment indicates that the paleointensities derived from the slopes of straight-line segments through the initial and highest temperature steps (prior to failures of pTRM checks) are very close to the correct (laboratory) field. In contrast, the lower (or higher) temperature data still yield erroneous paleointensity values that are too high (or too low; Fig. 14a), especially for sample RFA22252T. We recommend against selecting points on the NRM–TRM diagram that define the best straight line, or data that maximize the linear correlation coefficient (Fig. 14c).

High temperature VRM, cooling rates cannot explain the slight curvature (Fig. 14a) of the NRM–TRM plots and the higher than expected paleointensities (Fig. 14b) in the experiment involving the laboratory partial-TRM. This is perhaps more easily explained by PSD (or MD) grains (Kosterov and Prévot, 1998; Biggin and Thomas, 2003; Coe et al., 2003, 2004), than by some chemical changes.

If the large concave-up behaviors seen in the first Thellier experiment (Fig. 8a) were also due only to MD or PSD grains, the decrease in curvature of the NRM–TRM diagrams, during the second Thellier experiment, might be caused by transformation of some of these particules to SD-behaving particles caused by heating during the first experiments. However, hysteresis data on unheated and heated samples show only small changes (Fig. 15a), and the total TRM of the heated samples have slightly lower MDFs than the original NRMs. It is thus difficult to attribute

Fig. 15. (a) Comparison of hysteresis parameters for unheated (open symbols) and heated samples (black symbols) from Raiatea Island. Circles, sample RFA15157; diamonds, RFA222252; squares, RFA222249 (after Day et al., 1977). (b) Variations of low-field susceptibility versus temperature before and after the first Thellier experiment (sample RFA22245T) and before and after the second Thellier experiment (the other three samples). Arrows indicate the direction of temperature change.

the decrease in curvature to a shift in the particle size distribution to smaller more SD-behaving grains. However, the shapes of the *k–T* curves have changed slightly after the first or the second Thellier experiment (Fig. 15b). Theses changes might indicate minor chemical alteration of the magnetic carriers during the first heating.

The key observation for the samples in Fig. 8a and b and Fig. 14a, is that the lack of p-TRM acquisition in the lower temperature intervals seems to be compensated by p-TRMs acquired at higher temperatures (Fig. 14b).

The results of the two flows from Raiatea Island provide a good illustration for the need of measuring multiple samples from each unit. Despite their non-linear, concave-up curvature (Fig. 8a), we calculated paleointensity values from these samples in temperature intervals of successful pTRM checks and absence of CRM acquisition.

Six samples have a β (σ_b/b) factor lower than 0.1, which is used as a maximum value for selecting paleointensities by Selkin and Tauxe (2000) or Kissel and Laj (2004). Because of non-linearities, their quality factor, *q*, are considerably lower, and their contribution to the weighted mean "best estimate" paleointensity is less. These "lesser" samples provide consistency and add confidence in the value of the weighted mean, H_w. It is interesting to note in Fig. 8b and c that with increasing NRM fraction the paleointensity values converge to the results of the more linear samples. Therefore, samples showing curvature during paleointensity experiments (Table 3) need not be automatically rejected.

8. Conclusions

The goal of this work is to better understand factors that influence NRM–TRM diagrams obtained during Thellier experiments and ultimately to improve the accuracy and precision of paleointensity determinations by the Thellier TOP method.

Cooling-rate-dependence of TRM and high temperature VRM augment the initial primary NRM, arising from the slower initial cooling of the rock in nature versus the more rapid heating/cooling cycles during the laboratory experiments. This enhanced NRM can lead to overestimation of paleointensity determinations when only lower temperature data are considered. Also, paleointensity overestimation can result for PSD-MD particles, caused by the asymmetry of TRM acquisition and demagnetization, when only lower temperature data are considered.

Therefore:

1. We show that during Thellier experiments, the temperature interval chosen to calculate the paleointensity must include at least 40–50% of the NRM intensity. This criterion is in agreement with the study of Biggin and Thomas (2003). It should be considered for future studies and when evaluating published paleointensity results for calculating average geomagnetic field models.
2. It is better to increase the NRM fraction used in the paleointensity determination rather than use a lower NRM fraction to maximize the correlation coefficient of the selected line segment.
3. To assess the consistency of data from a single site, we propose merging the NRM–TRM data for all the samples from the particular site, with the TRM intensity normalized to a common laboratory field. When secondary remanences can be largely neglected, combining all the NRM–TRM data from a given site to a single Arai diagram is useful for detecting outlying data and samples (see Fig. 9).
4. The *R*-factor, which estimates the percentage of CRM acquisition (Coe et al., 1984), the MAD and DANG parameters (Selkin and Tauxe, 2000; Tauxe and Staudigel, 2004) provide similar information. We use an upper limit of 15% for *R* as a cutoff for selecting paleointensity data. Factor *q* (Coe et al., 1978) is a good estimate of the quality of the paleointensity determination, and we recommand to use it to weight individual results in calculating H_w.
5. Our results indicate that samples with mild or strong concave-up curvature of their NRM–TRM diagrams during paleointensity experiments need not be automatically rejected (see Fig. 8a and b). Such samples can provide useful paleointensity determinations, provided they are accompanied by successful pTRM checks and absence of CRM production. Paleointensity experiments should be continued to almost complete demagnetization of the NRM with adequate pTRM checks, so that the concave-up behavior can be recognized and

its origin assessed. If the complete behavior of the samples is not well determined, the use of lower (or higher) temperature interval might yield erroneous paleointensity values.

6. We consider that the best paleointensity value is provided by H_w, our "best estimate" (Table 3), which weights individual determinations by their quality factor. Consequently, samples with concave-up NRM–TRM diagrams will have lower q values and will contribute less to the H_w.
7. We introduce a site quality factor $Q = N\langle q\rangle$ to assess the comparative quality of paleointensity results from different cooling units.

Acknowledgments

We appreciated the technical support of the late Françoise Calza during this study. We thank Melina Macouin and the plaeomagnetic laboratory team of the CEREGE for help during hysteresis measurements. Reviews by M. Hill, N. Teanby, and an anonymous reviewer were greatly appreciated.

References

Abokhodair, A.A., 1977. The accuracy of the Thellier's technique for the determination of paleointensities of the Earth's magnetic field. Ph.D. Thesis, University of California, Santa Cruz, 346 pp.

Baag, C., Helsley, C.E., Xu, S., Lienert, B.R., 1995. Deflection of paleomagnetic directions due to magnetization of the underlying terrain. J. Geophys. Res. 100, 10013–10028.

Biggin, A.J., Böhnel, H.N., Zuniga, F.R., 2003. How many paleointensity determinations are required from a single flow to constitute a reliable average? Geophys. Res. Lett. 30 (11), 1575, DOI 10.1029.

Biggin, A.J., Thomas, D.N., 2003. The application of acceptance criteria to results of Thellier palaeointensity experiments performed on samples with pseudo-single-domain-like characteristics. Phys. Earth Planet. Inter. 138, 279–287.

Blais, S., Guille, G., Maury, R.C., Guillou, H., Miau, D., Cotten, J., 1997. Géologie et pétrologie de l'ile de Raiatea (Société, Plynésie française), série IIa. C. R. Acad. Sci. Paris t324, 435–442.

Calvo, M., Prévot, M., Perrin, M., Riisager, J., 2002. Investigating the reasons for the failure of palaeointensity experiments: a study on historical lava flows from Mt. Etna (Italy). Geophys. J. Int. 149, 44–63.

Coe, R.S., 1967. Determination of paleo-intensity of the Earth's magnetic field whith emphasis on mechanisms which could cause non-ideal behavior in Thellier's method. J. Geomagn. Geoelec. 25, 415–435.

Coe, R.S., Gromme, S., Mankinen, E.A., 1978. Geomagnetic paleointensities from radiocarbon-dated lava flows on Hawaii and the question of the Pacific nondipole low. J. Geophys. Res. 83, 1740–1756.

Coe, R.S., Gromme, S., Mankinen, E.A., 1984. Geomagnetic paleointensities from excursion séquences in lavas on Oahu, Hawaii. J. Geophys. Res. 89, 1059–1069.

Coe, R.S., Riisager, J., Plenier, G., 2003. Multidomain behavior in paleointensity experiments. Geophys. Res. Abstr. 5, 03052.

Coe, R.S., Riisager, J., Plenier, G., Leonhardt, R., Krása, D., 2004. Multidomain behavior during Thellier paleointensity experiments: results from the 1915 Mt. Lassen flow. Phys. Earth Planet. Int. 147, 141–153.

Chauvin, A., Gillot, P.Y., Bonhommet, N., 1991. Paleointensity of the Earth's magnetic field recorded by two late quaternary volcanic sequences at the island of La Reunion (Indian Ocean). J. Geophys. Res. 96, 1981–2006.

Chauvin, A., Garcia, Y., Lanos, Ph., Laubenheimer, F., 2000. Paleointensity of the geomagnetic field recovered on archaeomagnetic sites from France. Phys. Earth Planet. Int. 120, 111–136.

Day, R., Fuller, M., Schmidt, V.A., 1977. Hysteresis properties of titanomagnetites: grain-size and compositional dependence. Phys. Earth Planet. Int. 13, 260–267.

Dodson, M.H., McClelland, E., 1980. Magnetic blocking temperatures of single-domain grains during slow cooling. J. Geophys. Res. 85, 2625–2637.

Duncan, R.A., McDougall, I., 1976. Linear volcanism in French Polynesia. J. Volcanol. Geotherm. Res. 1, 197–227.

Dunlop, D., Özdemir, O., 1997. Rock Magnetism: Fundamentals and Frontiers. Cambridge University Press, Cambridge and New York, 573 pp.

Fabian, K., 2001. A theoretical treatment of paleointensity determination experiments on rocks containing pseudo-single or multi domains magnetic particules. Earth Planet. Sci. Lett. 188, 45–58.

Fox, J.M.W., Aitkin, M.J., 1980. Cooling-rate dependence of thermoremanent magnetization. Nature 283, 462–463.

Hill, M., Shaw, J., 2000. Magnetic field intensity study of the 1960 Kilauea lava flow, Hawaii, using the microwave palaeointensity technique. Geophys. J. Int. 142, 487–504.

Kissel, C., Laj, C., 2004. Improvements in procedure and paleointensity selection criteria (PICRIT-03) for Thellier and Thellier determinations: application to Hawaiian basaltic longcores. Phys. Earth Planet. Int. 147, 155–169.

Kosterov, A.A., Prévot, M., 1998. Possible mechanisms causing failure of Thellier palaeointensity experiments in some basalts. Geophys. J. Int. 134, 554–572.

Laj, C., Kissel, C., Scao, V., Beer, J., Thomas, D.M., Guillou, H., Muscheler, R., Wagner, G., 2002. Geomagnetic intensity and inclination variations at Hawaii for the past 98 Kyr from core SOH-4 (Big Island): a new study and a comparison with existing contemporary data. Phys. Earth Planet. Int. 129, 205–243.

Levi, S., 1977. The effect of magnetite particule size on paleointensity determinations of geomagnetic field. Phys. Earth Planet. Int. 13, 245–259.

Levi, S., Merrill, R.T., 1978. Properties of single-domain, pseudo-single-domain, and multidomain magnetite. J. Geophys. Res. 83, 309–323.

Mankinen, E.A., Champion, D.E., 1993. Broad trends in geomagnetic paleointensity on Hawaii during Holocene time. J. Geophys. Res. 98, 7959–7976.

Merrill, R.T., 1970. Low-temperature treatments of magnetization and magnetite-bearing rocks. J. Geophys. Res. 75, 3343–3349.

Perrin, M., Schnepp, 2004. IAGA paleointensity database: distribution and quality of the data set. Phys. Earth Planet. Int. 147, 255–267.

Prévot, M., Mankinen, E.A., Coe, R.S., Gromme, C.S., 1985. The Steens Mountain (Oregon) geomagnetic polarity transition. 2. Field intensity variations and discussion of reversal models. J. Geophys. Res. 90, 10417–10448.

Riisager, P., Riisager, J., 2001. Detecting multidomain magnetic grains in Thellier palaeointensity experiments. Phys. Earth Planet. Int. 125, 111–117.

Selkin, P.A., Tauxe, L., 2000. Long-term variations in palaeointensity. Phil. Trans. R. Soc. Lond. A 358, 1065–1088.

Shcherbakov, V.P., Shcherbakova, V.V., 2001. On the suitabillity of the Thellier method of palaeointensity determinations on pseudo-single-domain and multidomain grains. Geophys. J. Int. 124, 20–30.

Tanaka, H., Kono, M., 1991. Preliminary results and reliability of palaeointensity studies on historical and 14C dated Hawaiian lavas. J. Geomagn. Geoelect. 43, 375–388.

Tauxe, L., Staudigel, H., 2004. Strength of the geomagnetic field in the Cretaceous normal superchron: new data from submarine basaltic glass of the Troodos Ophiolite. Geochem. Geophys. Geosyst. 5, doi:10.1029/2003GC000635, Q02H06.

Thellier, E., Thellier, O., 1944. Recherches géomagnétiques sur des coulées volcaniques d'Auvergne. Ann. Geophys. 1, 34–42.

Thellier, E., Thellier, O., 1959. Sur l'intensité du champ magnétique terrestre dans le passé historique et géologique. Ann. Geophys. 15, 285–376.

Tsunakawa, H., Shaw, J., 1994. The Shaw method of palaeointensity determinations and its application to recent volcanic rocks. Geophys. J. Int. 118, 781–787.

Valet, J.P., 2003. Time variations in geomagnetic intensity. Rev. Geophys. 41 (1), 1004, doi:10.1029/2001RG000104.

Valet, J.P., Soler, V., 1999. Magnetic anomalies of lava fields in the Canary island. Possible consequences for paleomagnetic records. Phys. Earth Planet. Int. 115, 109–118.

Yamamoto, Y., Tsunakawa, H., Shibuya, H., 2003. Palaeointensity study of the Hawaiian 1960 lava: implications for possible causes of erroneously high intensities. Geophys. J. Int. 153, 263–276.

Yu, Y., Tauxe, L., Genevey, A., 2004. Toward an optimal geomagnetic field intenisty determination technique. Geochem. Geophys. Geosyst. 5, doi:10.1029/2003GC000630, Q02H07.